Pflügers Arch – Eur J Physiol (2000) 440:366–379
Digital Object Identifier (DOI) 10.1007/s004240000294

ORIGINAL ARTICLE

Virginijus Valiunas · Robert Weingart

Electrical properties of gap junction hemichannels identified in transfected HeLa cells

Received: 4 November 1999 / Received after revision and accepted: 11 February 2000 / Published online: 4 April 2000

Abstract Human HeLa cells transfected with mouse connexin Cx30, Cx46 or Cx50 were used to study the electrical properties of gap junction hemichannels. With no extracellular Ca^{2+}, whole-cell recording revealed currents arising from hemichannels. Multichannel currents showed a time-dependent inactivation sensitive to voltage, V_m. Plots of the instantaneous conductance, $g_{hc,inst}$, versus V_m were constant; plots of the steady-state conductance, $g_{hc,ss}$, versus V_m were bell-shaped. Single-channel currents showed two conductances, $\gamma_{hc,main}$ and $\gamma_{hc,residual}$, the latter ≅1/6 of the former. Single-channel currents exhibited fast transitions (1–2 ms) between the main state and residual state. Late during wash-in and early during wash-out of 2 mM heptanol, single-hemichannel currents showed slow transitions between an open state and closed state. The open channel probability, P_o, was V_m-dependent. It declined from ≅1 at V_m= 0 mV to 0 at large V_m of either polarity. Hemichannel currents showed a voltage-dependent $\gamma_{hc,main}$, i.e., it increased/decreased with hyperpolarization/depolarization. Extrapolation to V_m=0 mV led to a $\gamma_{hc,main}$ of 283, 250 and 352 pS for Cx30, Cx46 and Cx50, respectively. The hemichannels possess two gating mechanisms. Gating with positive voltage reflects V_j-gating of gap junction channels, gating with negative voltage reflects a property inherent to hemichannels, i.e., V_m or "loop" gating. We conclude that Cx30, Cx46 and Cx50 form voltage-sensitive hemichannels in single cells which are closed under physiological conditions.

V. Valiunas · R. Weingart (✉)
Department of Physiology, University of Bern,
Bühlplatz 5, 3012 Bern, Switzerland
e-mail: WEINGART@PYL.UNIBE.CH
Tel.: +41-31-6318711, Fax: +41-31-6314611

V. Valiunas
Institute for Biomedical Research, Kaunas Medical University,
Eiveniu 4, 3007 Kaunas, Lithuania

V. Valiunas
Department of Physiology and Biophysics,
Health Science Center, SUNY at Stony Brook,
Stony Brook NY 11794–8661,USA

Key words Connexin30 · Connexin46 · Connexin50 · Electrophysiology · Gap junction · Hemichannel

Introduction

Gap junctions constitute assemblies of intercellular channels. Each channel consists of two hemichannels (connexons) composed of six transmembrane proteins (connexins, Cx). They offer an aqueous pathway for the exchange of intracellular ions and small molecules. So far, more than 13 connexins have been identified in vertebrate cells encoded by a multi-gene family [2]. This makes it possible to form homotypic (both connexons consist of same connexin type), heterotypic (each connexon consists of different connexin type) and heteromeric channels (each connexon composed of more than one connexin type). Oligomerization of connexins into hemichannels occurs prior to entry into the Golgi [12]. Docking of hemichannels to gap junction channels involves non-covalent interactions [13] and results in the formation of leak-free intercellular channels [4]. Gap junctions are dynamic structures whose channels are continuously replaced (see [2]).

Over the last decade, cell pairs have been used extensively to examine the electrical properties of gap junction channels. From these studies a generalized picture emerged describing the operation of the channels [2, 26]. Under physiological conditions, gap junction channels are usually open. In the presence of transjunctional voltages and chemical uncoupling agents, they undergo partial and complete closure, respectively [4]. In contrast, hemichannels embedded in cell membranes are normally closed. However, as shown recently, they can open when the resting potential and/or the extracellular Ca^{2+} concentration is reduced. Evidence for the existence of hemichannels was first obtained from electrical studies of horizontal cells of fish retina [6, 16]. Similar observations were then made in studies of *Xenopus* oocytes expressing identified connexins. Injection of mRNA for rat Cx46 or chicken Cx56 induced currents attributable to

hemichannels [10, 11]. Later on it was shown that Cx38, the intrinsic connexin of *Xenopus* oocytes, also forms hemichannels [9]. Recently it was demonstrated that injected *Xenopus* oocytes are suitable for studying single hemichannels [22].

The aim of the present study has been to establish a system that allows us to investigate the electrical properties of hemichannels in vertebrate cells. We used human HeLa cells transfected with rat Cx30, Cx46 or Cx50. The measurements were performed with a voltage-clamp method and patch pipettes. The main emphasis was on channel conductance and voltage gating. The experiments on hemichannels complement previous studies of gap junction channels. Hence, they lead to a better understanding of gap junction channel properties. Preliminary results are published elsewhere [23].

Materials and methods

Cells and culture conditions

Wild-type and transfected HeLa cells expressing mouse Cx30, Cx46 or Cx50 (C. Elfgang, S. Haubrich, K. Willecke, work in preparation; [25] were grown in Dulbecco's medium (DMEM) containing 10% fetal calf serum (FCS), 100 µg/ml streptomycin and 100 U/ml penicillin. Transfected cells were selected using 0.5–1 µM Puromycin (Sigma). To perform experiments, the cells were harvested, suspended in DMEM with 10% FCS ($\cong 0.2 \cdot 10^6$–$1 \cdot 10^6$ cells/ml) and seeded onto sterile glass coverslips placed in multiwell culture dishes ($\cong 10^4$ cells/cm^2).

Solutions and pipettes

Experiments were carried out with the cells bathed in Krebs-Ringer solution containing (mM): NaCl, 140; KCl, 4; $CaCl_2$, 2; $MgCl_2$, 1; HEPES, 5 (pH 7.4); glucose, 5; pyruvate, 2. Patch pipettes were pulled from glass capillaries (GC150TF-10; Clark Electromedical Instruments, Pangbourne, UK) by means of a horizontal puller (DMZ-Universal; Zeitz Instruments, Augsburg, Germany). Unless stated, patch pipettes were filled with solution containing (mM): potassium aspartate, 120; NaCl, 10; $CaCl_2$, 1; $MgCl_2$, 1; MgATP, 3; HEPES, 5 (pH 7.2); EGTA, 10 (pCa≅8); filtered through 0.22-µm pores. When filled the pipettes had DC resistances of 3–5 MΩ. SKF-525A (Proadifen; Biomol Research Laboratories, Plymouth Meeting, Pa., USA) or *n*-heptanol was dissolved directly in Krebs-Ringer solution.

Electrical measurements

The experimental chamber was mounted on the stage of an inverted microscope equipped with phase-contrast optics (Diaphot-TMD, Nikon; Nippon Kogaku, Tokyo, Japan). The chamber was perfused with Krebs-Ringer solution at room temperature (22–26°C). Coverslips with adherent cells were transferred to the chamber. Experiments were carried out on single cells using a single voltage-clamp. A selected cell was attached to a patch pipette connected to a micromanipulator (WR-88; Narishige Scientific Instrument, Tokyo, Japan) and an amplifier (EPC 7; List Electronic, Darmstadt, Germany). This method permitted us to control the membrane potential ($V_{m)}$ and measure the associated current (I_m) [4].

Signal recording and analysis

Voltage and current signals were pulse-code modulated and recorded on videotape (DR-886; Neuro Data Instruments, New York, N.Y., USA). For off-line analysis with a PC, the current signals were filtered at 1 kHz (–3 dB) with an 8-pole Bessel filter (902LPF; Frequency Devices, Haverhill, Mass., USA) and digitized at 3.33 kHz with a 12-bit A/D converter (IDA 12120; INDEC Systems, Capitola, Calif., USA). Data acquisition and analysis were performed with modular (C-Lab; INDEC Systems) and custom-made software [15]. The results are presented as means ±1SEM. Curve fitting and statistical analyses were done with SigmaPlot and SigmaStat, respectively (Jandel Scientific, Erkrath, Germany).

Results

Hemichannel currents in transfected HeLa cells

HeLa cells transfected with cDNA of rat Cx30, Cx46 or Cx50 express functional gap junction channels as shown by cell pair experiments ([25] V. Valiunas and R. Weingart, unpublished observations; R. Sakai, C. Elfgang, K. Willecke, R. Weingart, work in preparation). Using the induced cell pair approach [4], we observed de novo formation of gap junction channels in some cases. This suggests that silent hemichannels are present in cell membranes of transfected cells.

Figure 1 illustrates the procedure used to elicit putative hemichannel currents. The records were gained from a Cx46-HeLa cell superfused with Krebs-Ringer solution. After establishing the whole-cell recording conditions, V_m was clamped to –20 mV. Voltage pulses were then delivered to depolarize V_m to 5, 30 and 55 mV (V_m traces). In the presence of 2 mM extracellular Ca^{2+}, this elicited a small outward current, I_m. It increased with depolarization but showed no time dependence (Fig. 1A); hence, it was presumably carried by K^+ [7]. In the absence of Ca^{2+}, this protocol provoked large outward currents that increased with depolarization and were time dependent (Fig. 1B). Depolarization also increased the fluctuations of I_m suggesting the involvement of channels with significant conductance, conceivably hemichannels. Using this procedure, we obtained similar results with HeLa cells expressing Cx30 or Cx50 (data not shown). In contrast, wild-type HeLa cells exposed to solution with no Ca^{2+} (Fig. 1C) yielded I_m signals comparable to those in Fig. 1A. These observations are consistent with the notion that the extra I_m in Ca^{2+}-free solution is mediated by channels present after transfection, i.e., hemichannels.

We have also examined the effects of inorganic ions on the extra I_m. It turns out that 2 mM Cs^+, Ba^{2+} or tetraethylammonium (TEA^+) in the extracellular solution does not block the current evoked in Ca^{2+}-free solution. This is consistent with the involvement of hemichannels. Thus, we tentatively conclude that the Ca^{2+}-sensitive I_m reflects current flow through hemichannels and hence we named it I_{hc} (hc: hemichannel).

Voltage dependence of hemichannel currents

Figure 2 illustrates an experiment that explored the V_m sensitivity of I_{hc}. A Cx30-HeLa cell was first exposed to

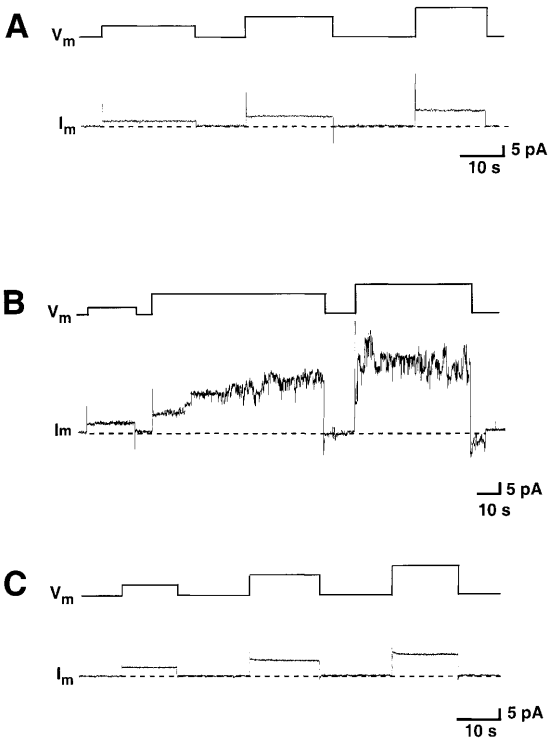

Fig. 1A–C Currents elicited in a HeLa cell expressing connexin46 (*Cx46*). Starting from –20 mV, the membrane potential, V_m, was depolarized in steps to elicit outward currents of growing amplitude, I_m. *A* I_m responses recorded in Krebs-Ringer solution with 2 mM Ca^{2+}. V_m was depolarized to 5, 30 and 55 mV. **B** I_m responses recorded in solution with no added Ca^{2+}. This induced an extra current component with a time-dependent activation, attributable to hemichannels. V_m was depolarized to 5, 30 and 55 mV. **C** I_m responses in a wild-type HeLa cell recorded in Ca^{2+}-free solution. V_m was depolarized to 5, 30 and 55 mV

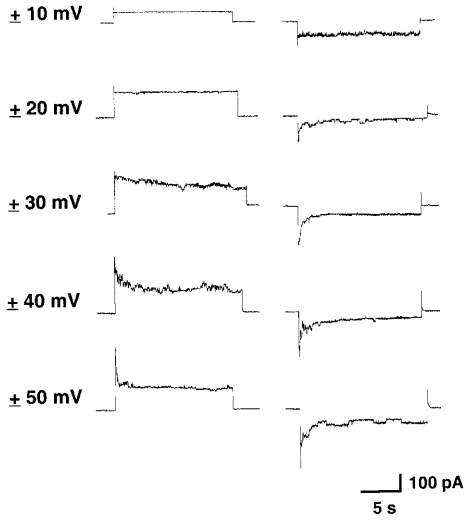

Fig. 2 Multi-hemichannel currents, I_{hc}, determined in a Cx30-HeLa cell. Family of current traces elicited by depolarizing (*left hand column*) and hyperpolarizing voltage pulses (*right hand column*) of growing amplitude. At small V_m, I_{hc} remained virtually constant during the pulse. At large V_m, after an initial peak at the onset of the pulse ($I_{hc,inst}$; inst: instantaneous), I_{hc} decayed with time to reach a stable level ($I_{hc,ss}$; ss: steady state). Bath: Krebs-Ringer solution with no added Ca^{2+}, NaCl replaced by KCl

Krebs-Ringer solution. After establishing the whole-cell recording conditions, it was superfused with Ca^{2+}-free saline whose NaCl had been replaced by KCl. Starting from a holding potential of 0 mV, voltage pulses were then applied to change V_m in increments of 2.5–10 mV. Figure 2 shows a family of I_{hc} traces elicited by depolarizing (left hand side) and hyperpolarizing (right hand side) pulses. At V_m up to 20 and –10 mV, I_{hc} increased in size but remained constant in time. At larger V_m, after an initial peak at the onset of the pulse, $I_{hc,inst}$ (inst: instantaneous), the current decayed with time to reach a stable level at the end of the pulse, $I_{hc,ss}$ (ss: steady state). With regard to speed and extent, the decay was more prominent at larger $|V_m|$.

The signals in Fig. 2 and others from the same experiment were analyzed to obtain the relationships $I_{hc}=f(V_m)$. To distinguish between capacitive and ionic currents at the beginning of each record, the signals were displayed at a fast time resolution. As shown in Fig. 3A, $I_{hc,inst}=f(V_m)$ (o) was virtually linear over the voltage range examined, i.e., ±50 mV. In contrast, $I_{hc,ss}=f(V_m)$ (•) deviated strongly from linearity at larger values of V_m. $I_{hc,ss}$ did not decline to zero even at large V_m.

Figure 3B shows plots of normalized conductances, i.e., $g_{hc,inst}$ versus V_m (o) and $g_{hc,ss}$ versus V_m (•). Individual values were obtained from the ratios $I_{hc,inst}/V_m$ and $I_{hc,ss}/V_m$, respectively. The $g_{hc,inst}$ data followed a straight line equivalent to a slope conductance of 7.2 nS. In contrast, the $g_{hc,ss}$ data followed a bell-shaped relationship which was asymmetrical. The decay of $g_{hc,ss}$ was more pronounced at negative voltages. At V_m larger than –12.5 mV or 20 mV, $g_{hc,ss}$ decreased steeply to a minimum different from zero. The smooth curve represents the best fit of data to the Boltzmann equation

$$\frac{g_{hc,ss}}{g_{hc,inst}} = \frac{1-g_{hc,min}}{1+e^{[A\cdot(V_m-V_{m,0})]}} + g_{hc,min} \quad (1)$$

where $g_{hc,min}$ is the minimal conductance at large V_m and $V_{m,0}$ corresponds to V_m at which $g_{hc,ss}/g_{hc,inst}$ is half-maximally inactivated. *A* is a constant which expresses gating charge, $zq(kT)^{-1}$, where *z* is the equivalent number of unitary positive charges *q* moving through the electric field applied, and *k* and *T* are the Boltzmann constant and the temperature in Kelvin, respectively. The analysis yielded the following values: $V_{hc,0}$=–14.9/27.7 mV, $g_{hc,max}$=0.99/1.0, $g_{hc,min}$=0.16/0.39, *z*=25/19 for negative/positive V_m. The relationships in Fig. 3A,B are reminiscent of gap junctions studied in cell pairs (see e.g., [4]). Averaging the data from five HeLa cells expressing Cx30, $g_{hc,inst}$ turned out to be 6.0±1.2 nS.

Figure 3C shows the analysis of an experiment carried out on a wild-type HeLa cell in saline with no added Ca^{2+}. The instantaneous (o) and steady-state currents (•) were virtually linear and superimposed. The analysis yielded an identical slope conductance, i.e., 0.15 nS. The average of five cells was 0.35±0.12 nS.

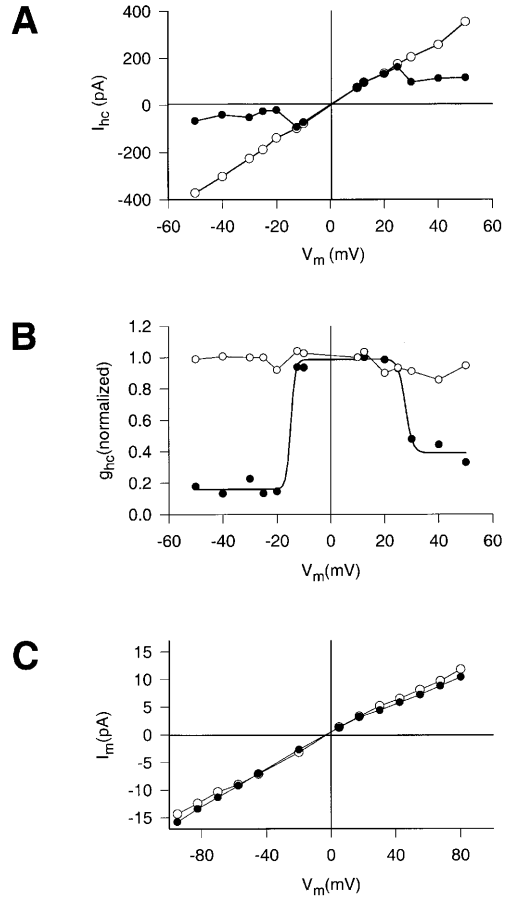

Fig. 3A–C Dependence of hemichannel conductance, g_{hc}, on voltage, V_m, determined in a Cx30-HeLa cell. *Symbols* correspond to single determinations. **A** Plots of $I_{hc,inst}$ (o) and $I_{hc,ss}$ (•) versus V_m. The function $I_{hc,inst}$=f(V_m) was virtually linear. Its slope equals a conductance, $g_{hc,inst}$, of 7.21 nS. The function $I_{hc,ss}$=f(V_{hc}) deviated strongly from linearity for |V_m|>–12.5 mV and 20 mV. **B** Plots of hemichannel conductances $g_{hc,inst}$ (o) and $g_{hc,ss}$ (•) versus V_m. *Smooth curve*: best fit of data to the Boltzmann equation ($V_{hc,0}$=–14.9/27.7 mV, $g_{hc,max}$=0.99/1.0, $g_{hc,min}$=0.16/0.39, z=25/19 for negative/positive V_m). **C** Plots of $I_{hc,inst}$ (o) and $I_{hc,ss}$ (•) versus V_m, determined in a wild-type HeLa cell. Note the different scales in **A** and **C**. Bath: Krebs-Ringer solution with no added Ca^{2+}, NaCl replaced by KCl

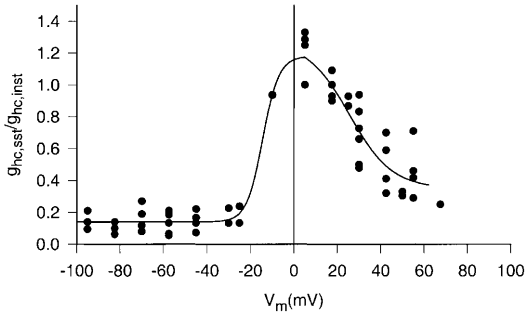

Fig. 4 Dependence of normalized conductance of Cx30 hemichannels at steady state, $g_{hc,ss}$, on membrane potential, V_m. Summary from five cells. *Symbols* correspond to single determinations. *Smooth curve*: best fit of data to the Boltzmann equation ($V_{hc,0}$=–14.3/25.6 mV, $g_{hc,max}$=1.18/1.27, $g_{hc,min}$=0.14/0.35, z=6.9/2.6 for negative/positive V_m). Bath: Krebs-Ringer solution with no added Ca^{2+}, NaCl replaced by potassium aspartate

Figure 4 summarizes results from five Cx30-HeLa cells studied under different ionic conditions. In these experiments the pipette solution and bath solution contained potassium aspartate instead of KCl and NaCl, respectively. These conditions are identical to those previously used to examine Cx30 gap junctions and hence allow direct comparisons [25]. The graph shows that the plot $g_{hj,ss}$=V_m was also asymmetrical. The analysis yielded the following parameters: $V_{hc,0}$=–14.3/25.6 mV, $g_{hc,max}$=1.18/1.27, $g_{hc,min}$=0.14/0.35, z=6.9/2.6 for negative/positive V_m.

Multichannel versus single-channel currents

Figure 5 compares multichannel and single-channel currents through Cx30 hemichannels. The cell was superfused with Ca^{2+}-free Krebs-Ringer solution. Figure 5A shows currents elicited with a biphasic pulse protocol, displayed at low magnification and a compressed time scale. Starting from a holding potential of –20 mV, V_m was first depolarized and then hyperpolarized by 25, 37.5, 50 and 62.5 mV (from left to right). This induced an outward current followed by an inward current. On the one hand, the sequence of depolarizations first gave rise to a time-dependent increase in $I_{hc,ss}$ and then to a decrease. The transition from activation to inactivation may reflect a change in open channel probability. On the other hand, the sequence of hyperpolarizations led to a gradual increase in $I_{hc,inst}$. At the same time, its inactivation grew progressively faster.

Figure 5B shows a current signal displayed at high magnification and an expanded time scale (lower traces), evoked by *depolarization* from –20 to 30 mV (upper trace). After a capacitive spike, the outward I_{hc} revealed discrete steps indicating the sequential opening of hemichannels (channel opening: upward deflections). Hence, the time-dependent increase of I_{hc} associated with depolarization in Fig. 5A is caused by *activation* of hemichannels. The current steps reflect transitions between the residual state and main state of a channel (see below). They were of comparable amplitude and correspond to conductance steps of 250–280 pS.

Figure 5C shows a current signal displayed at high magnification and an expanded time scale (lower trace), induced by *hyperpolarization* from –20 to –70 mV (upper trace). The inward I_{hc} revealed discrete steps indicative of sequential closure of hemichannels (channel opening: downward deflections). Thus, the time-dependent decrease of I_{hc} in Fig. 5A associated with hyperpolarization of V_m is brought about by *inactivation* of hemichannels. The analysis yielded conductance steps of 295–325 pS for the transitions between main states and residual states.

Comparison of currents from single Cx30, Cx46 and Cx50 hemichannels

Transfected HeLa cells often showed I_{hc} signals from tens of hemichannels. They were used to examine multi-

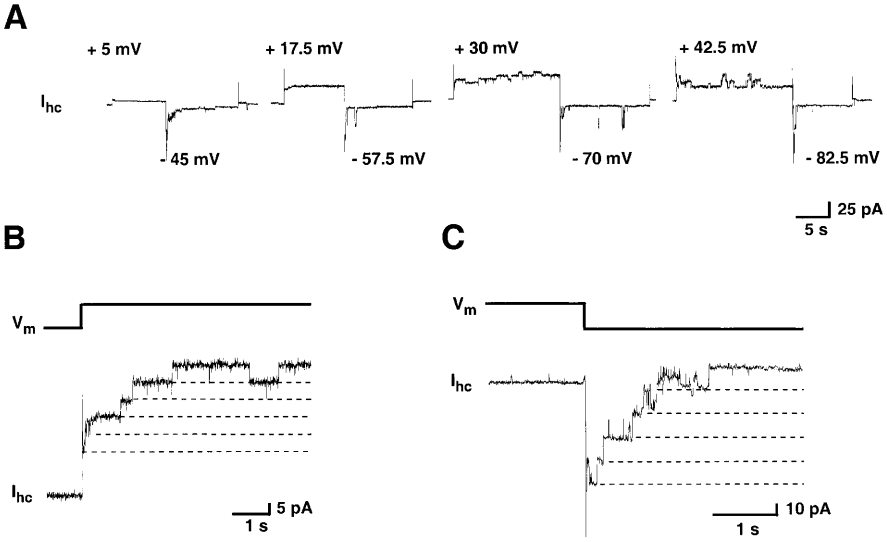

Fig. 5A–C Multi versus single hemichannel currents, I_{hc}, gained from a Cx30-HeLa cell. **A** Multichannel I_{hc} displayed at low magnification and on a compressed time scale, elicited by symmetrical biphasic pulses. Holding potential: –20 mV. **B** Single-channel I_{hc} displayed at high magnification and expanded time scale (*lower trace*), elicited by depolarization from –20 to 30 mV (*upper trace*). I_{hc} shows discrete steps indicative of the sequential opening of hemichannels. The current steps yielded a conductance of 250–280 pS attributable to transitions between the main state and residual state. **C** Single-channel I_{hc} displayed at high magnification and on an expanded time scale (*lower trace*), induced by hyperpolarization from –20 to –70 mV (*upper trace*). I_{hc} showed discrete steps indicative of sequential closure of hemichannels. The current steps yielded a conductance of 295–325 pS. Bath: Krebs-Ringer solution with no added Ca^{2+}

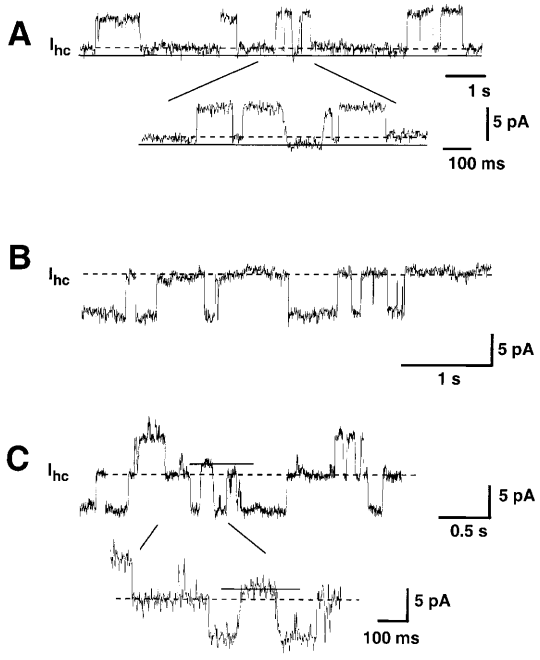

Fig. 6A–C Comparison of single hemichannel currents, I_{hc}. **A** Cx50-HeLa cell with V_m maintained at 50 mV (channel opening: *upward deflections*). I_{hc} mainly flickered between two levels attributable to the main state and residual state (*dotted line*). *Solid line*: zero current. *Inset*: I_{hc} segment displayed on an expanded time scale. It shows fast transitions between channel open states (i.e., main state and residual state) and slow transitions involving the closed state. **B** Cx46-HeLa cell with V_m held at –20 mV (channel opening: *downward deflections*). **C** Cx30-HeLa cell with V_m set to –20 mV (channel opening: *downward deflections*). *Inset*: I_{hc} segment at an expanded time scale exhibiting fast and slow transitions. Bath: Krebs-Ringer solution with no added Ca^{2+}

hemichannel currents. In some cells, I_{hc} decreased gradually with time due to loss of hemichannels. Once the number of operational hemichannels was three or less, these cells were suitable for studying single hemichannels. In some cases, this process was accelerated by exposure to 75 µM SKF-525A, a lipophilic agent which reversibly blocks gap junction channels without affecting conductance [21].

Figure 6 compares single hemichannel currents from HeLa cells expressing different connexins. Figure 6A shows an example of a Cx50 hemichannel. The cell was exposed to Ca^{2+}-free Krebs-Ringer solution while V_m was maintained at 50 mV. The upper trace shows a current segment at compressed time scale (channel opening: upward deflections). I_{hc} preferentially flickered between two discrete levels attributable to the main state and residual state (dotted line). The solid line marks zero current. The lower trace repeats a short portion of I_{hc} at an expanded time scale. It reveals two types of transitions, fast ones with transition times shorter than 1 ms (approx. frequency response of experimental setup) and slow ones with transition times of 17–25 ms. The fast transitions involved the main state and residual state (i.e., channel open states) and were frequently observed. The slow transitions occurred between an open state and the closed state and were rarely seen. Hence, the residual state may be regarded as the ground state for fast transitions and the closed state as ground state for slow transitions. The analysis yielded the following conductances: $\gamma_{hc,main}$=260 pS, $\gamma_{hc,residual}$=43 pS.

Figure 6B shows an example of a Cx46 hemichannel. The cell was superfused with Ca^{2+}-free Krebs-Ringer solution while V_m was maintained at –20 mV (channel opening: downward deflections). The compressed current segment indicates that I_{hc} mainly flickered between the main state and residual state (dotted line). On rare occasions, it exhibited slow transitions involving the channel closed state (data not shown). The analysis yielded conductance steps of 262–285 pS corresponding to transitions between the main state and residual state.

Figure 6C shows an example of a Cx30 hemichannel. The experimental conditions were identical to those in Fig. 6B. Two channels were active in this case (channel opening: downward deflections). The upper trace displays a current segment at a compressed time scale. The channels mostly flickered between the main state and the residual state. The dotted line corresponds to $I_{hc,main}$(channel 1)+$I_{hc,residual}$(channel 2); the solid line corresponds to $I_{hc,main}$(channel 1), i.e., the second channel was closed completely. The lower trace repeats a portion of I_{hc} at an expanded time scale. It reveals fast transitions between the main state and residual state and slow ones between the main state and closed state. The analysis yielded the following conductances: $\gamma_{hc,main}$=370 pS, $\gamma_{hc,residual}$=67 pS.

On rare occasions, single-channel currents from Cx30, Cx46 or Cx50 cells exhibited short events interposed between the main state and residual state (see Fig. 6). Conceivably, they represent channel substates (see below).

Hemichannel activity in the cell-attached mode

The data presented so far were gained with the whole-cell recording mode. However, single hemichannel currents were also seen in the cell-attached patch mode. Figure 7 illustrates records obtained from two Cx30-HeLa cells at 36°C. The cells were exposed to Ca^{2+}-free Krebs-Ringer solution whose NaCl had been replaced by KCl.

Hence, the patch potential, V_{patch}, was inversely proportional to the pipette potential, V_{pip} (V_{patch}=V_m–V_{pip}). The upper and lower traces show an example with one and two channels, respectively. In the former case, V_{pip} was stepped from 30 to –20 mV. First the channel was fully closed (solid line). After some delay, it opened and I_{hc} began to flicker between two prominent levels corresponding to the main state and residual state (dashed line). The analysis yielded the following conductances: $\gamma_{hc,main}$=428 pS, $\gamma_{hc,residual}$=72 pS. In the latter case, V_{pip} was maintained at –20 mV. I_{hc} exhibited three major levels corresponding to $I_{hc,residual}$ (dashed line), $I_{hc,main}$+ $I_{hc,residual}$, and 2·$I_{hc,main}$. The analysis yielded conductance jumps of 326–344 pS. Both current traces showed few events of short lifetime interposed between the main state and residual state, presumably reflecting substates. Towards the end of the experiments, the membrane patches were disrupted. This revealed an V_m of 0 and –1 mV, respectively.

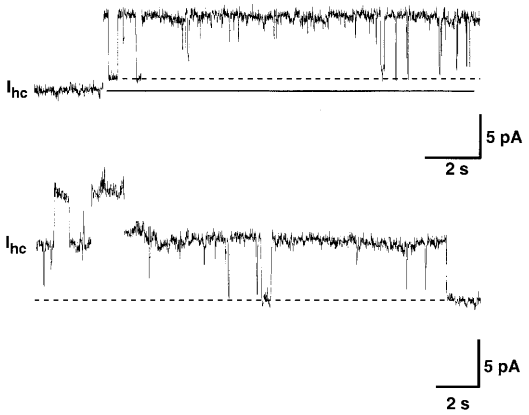

Fig. 7 Hemichannel currents, I_{hc}, from a Cx30-HeLa cell, gained in the cell-attached patch configuration. Examples with a single channel (*upper trace*) and two channels (*lower trace*). I_{hc} was elicited by a V_{patch} of 20 mV (channel opening: *upward deflections*). *Dashed lines*: residual current; *solid line*: zero current. Bath: Krebs-Ringer solution with no added Ca^{2+}, NaCl replaced by KCl. Temperature: 36°C

Chemical gating of hemichannels

Long-chain alkanols reversibly block gap junction channels [28]. This property was used to further characterize I_{hc} in Cx30-HeLa cells. The measurements were carried out with Ca^{2+}-free Krebs-Ringer solution containing KCl instead of NaCl. Figure 8A, B illustrates the effect of 3 mM heptanol on multichannel currents evoked by a bipolar pulse. Starting from a holding potential of –20 mV, V_m was first depolarized and then hyperpolarized by 50 mV. During control (Fig. 8A), this produced an outward current increasing with time and an inward current decreasing with time, reflecting activation and inactivation of I_{hc}, respectively. The inset repeats the initial current segment on an expanded time scale (see brackets) to document the time-dependent increase in I_{hc}. In the presence of heptanol (Fig. 8B), the time-dependent components of I_{hc} were completely blocked. The remaining currents resembled those seen in transfected or wild-type HeLa cells in normal Krebs-Ringer solution (see Fig. 1A,C). I_{hc} recovered completely after washout of heptanol (not shown). These observations support the view that I_{hc} is carried by hemichannels.

Figure 8C, D illustrates the effects of 2 mM heptanol on single-channel currents. A Cx30-HeLa cell was superfused with Ca^{2+}-free solution containing KCl instead of NaCl. Currents were measured at a maintained V_m of 30 mV. Following a short control period, the lipophilic agent was gently washed in. After complete inhibition of I_{hc}, it was slowly washed out again. This provoked a sequential block of hemichannels followed by a sequential recovery. Late during wash in of heptanol, I_{hc} exhibited slow transitions between current levels corresponding to the main state and closed state (Fig. 8C). They terminated fast flickering between the main state and residual state (dotted line). To emphasize this aspect, the insets repeat current segments on an expanded time scale (see

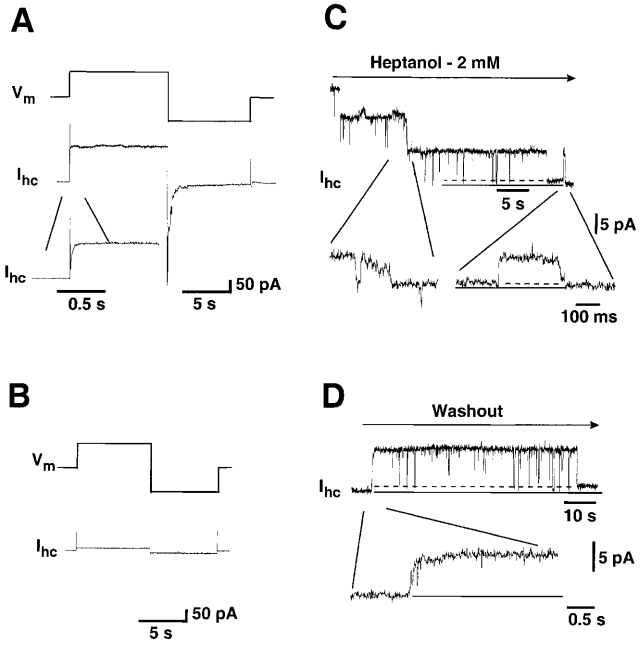

Fig. 8A–D Chemical gating examined in Cx30-HeLa cells. **A**, **B** Multichannel currents. Starting from –20 mV, V_m was depolarized and hyperpolarized by 50 mV (*upper traces*). This evoked an outward and inward I_{hc}, respectively (*lower traces*). During control (**A**), the outward/inward I_{hc} increased/decreased with time reflecting activation/inactivation of hemichannels. *Inset*: initial I_{hc} segment at an expanded time scale showing a capacitative spike followed by a time-dependent increase of inward current. In the presence of 2 mM *n*-heptanol (**B**), the time-dependent currents were blocked. **C**, **D** Single-channel currents. Wash in of alkanol (**C**) provoked a gradual decrease in I_{hc} caused by sequential channel block. During this process, I_{hc} exhibited slow transitions between the main state and closed state (see *insets*). Washout of alkanol (**D**) led to a gradual increase in I_{hc} brought about by sequential recovery of blocked channels. During this process, the channels resumed their activity with a slow transition between the closed state and main state (see *inset*). V_m=30 mV. *Dotted lines*: residual current; *solid lines*: zero current. Bath: Krebs-Ringer solution with no added Ca^{2+}, NaCl replaced by KCl

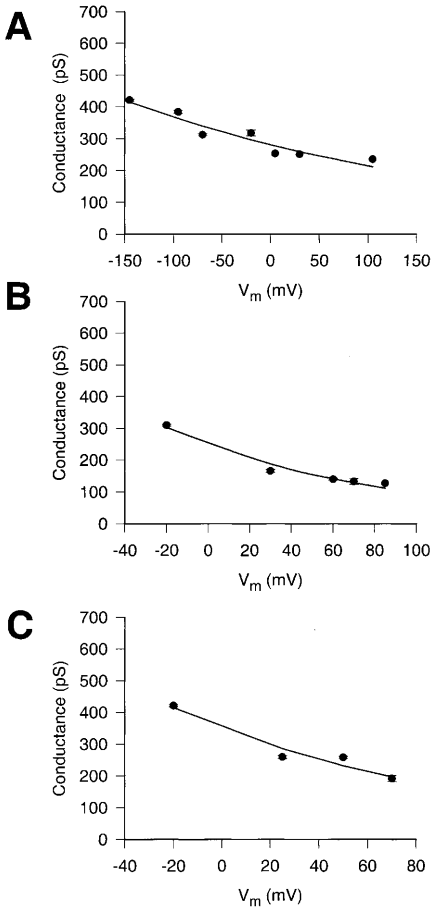

Fig. 9A–C Voltage dependence of single hemichannel conductances, $\gamma_{hc,main}$. Values of $\gamma_{hc,main}$ were averaged and plotted versus V_m. *Symbols* represent mean values ±1SEM. Curves correspond to the best fit of data to an exponential (for details, see text). **A** Cx30 hemichannel data gained from four cells. $\Gamma_{hc,main}$=283 pS, V_H=–373 mV. **B** Cx46 hemichannel data obtained from three cells. $\Gamma_{hc,main}$=250 pS, V_H=–108 mV. **C** Cx50 hemichannel data gathered from four cells. $\Gamma_{hc,main}$=352 pS, $V_{m,0}$=–121 mV. Bath: Krebs-Ringer solution with no added Ca^{2+}

brackets). Early during washout of heptanol, a first channel resumed its activity with a slow transition between the closed state and main state (Fig. 8D, see inset). Subsequently, it started to flicker with fast transitions between the main state and residual state. The polarity of V_m had no influence on these phenomena (data not shown). The succession of events late during uncoupling and early during recovery from uncoupling are reminiscent of chemical gating of gap junction channels [24]. Hence, Fig. 8C, D is consistent with the view that I_{hc} is attributable to hemichannel currents. Similar results were obtained with HeLa cells expressing Cx46 or Cx50 hemichannels.

Voltage dependence of hemichannel conductance

We have also explored the relationship between hemichannel conductance and V_m. For this purpose, $\gamma_{hc,main}$ was determined using voltage pulses of different amplitude and either polarity. The experiments were carried out using Ca^{2+}-free Krebs-Ringer solution. The data were sampled, averaged and plotted versus V_m. Figure 9A summarizes the complete results from four Cx30-HeLa cells. Over the voltage range examined, i.e., –145 to 100 mV, $\gamma_{hc,main}$ was dependent on V_m. It increased with hyperpolarization and decreased with depolarization. The solid curve represents the best fit of data to the exponential:

$$\gamma_{hc,main} = \Gamma_H \cdot e^{-\frac{V}{V_H}} \quad (2)$$

where Γ_H corresponds to the conductance at V_m=0 mV and V_H is the decay constant at which $\gamma_{hc,main}$ declines to e^{-1}. The analysis yielded the following values: Γ_H=283 pS, V_H=–373 mV (see [26]). For comparison, the conductance of Cx30 gap junction channels, $\gamma_{j,main}$, was found to be

141 pS at 23°C [25]. Figure 9B summarizes the complete results from three Cx46-HeLa cells. In these experiments, V_m was altered from –20 to 85 mV. Like for Cx30, $\gamma_{hc,main}=f(V_m)$ was non-linear. The solid curve corresponds to the best fit of data to Eq. 2. The analysis revealed the following values: Γ_H=250 pS, V_H=–108 mV. For comparison, the $\gamma_{j,main}$ of Cx46 gap junction channels was reported to be 120 pS [calculated for 23°C; (R. Sakai, C. Elfgang, K. Willecke, R. Weingart, work in preparation)]. Figure 9C summarizes the data from four Cx50-HeLa cells. In this series of experiments, V_m was stepped from –20 to 70 mV. As for Cx30 and Cx46, $\gamma_{hc,main}=f(V_m)$ was non-linear. Fitting of the data to Eq. 2 (solid curve) yielded the following parameters: Γ_H=352 pS, V_H=–121 mV. For comparison, $\gamma_{j,main}$ of Cx50 gap junction channel was estimated as 203 pS at 23°C (V. Valiunas and R. Weingart, unpublished).

Influence of temperature on hemichannel conductance

Next we examined the effect of temperature on the $\gamma_{hc,main}$ of Cx30 hemichannels. The temperature in the experimental chamber was controlled with a Peltier element and a thermistor [3]. The protocol involved application of long V_m pulses (–20 or 30 mV) and assessment of I_{hc}. The experiments were carried out in Ca^{2+}-free Krebs-Ringer solution. Figure 10A shows I_{hc} records obtained at 22°C (upper trace) and 36°C (lower trace) elicited at V_m=–20 mV. The analyses yielded conductances of 320–334 pS and 460–486 pS, respectively. The $\gamma_{hc,main}$ values were sampled, averaged and plotted versus temperature, *T*, as shown in Fig. 10B. Over the temperature range examined, i.e., 22–36°C, $\gamma_{hc,main}$ increased with increasing temperature at V_m=–20 mV (•) and V_m=30 mV (o). The solid lines were obtained by fitting the data to the equation:

$$\gamma_{hc,main}(T) = \gamma_{hc,main}(22) \cdot Q_{10}^{[(T-22)/10]} \quad (3)$$

where $\gamma_{hj,main}(22)$ is the conductance at 22°C and Q_{10} the temperature coefficient. Q_{10} turned out to be 1.28 (n=30) for V_m=–20 mV and 1.25 (n=39) for V_m=30 mV, respectively. This suggests that the Q_{10} of $\gamma_{hj,main}$ is V_m-insensitive.

Open-state probability

Cx30-HeLa cells with a single operational hemichannel were used to study channel kinetics. As shown above (see Fig. 6), I_{hc} flickers between $I_{hc,main}$ and $I_{hc,residual}$. Hence, the analysis of long records allows us to explore the open-state probability, P_o, at steady state. The protocol involved establishing V_m gradients of different amplitude (–45 to 50 mV) and long duration (>15 s). The initial segment of I_{hc} records was discarded to avoid interference from time-dependent activation or inactivation.

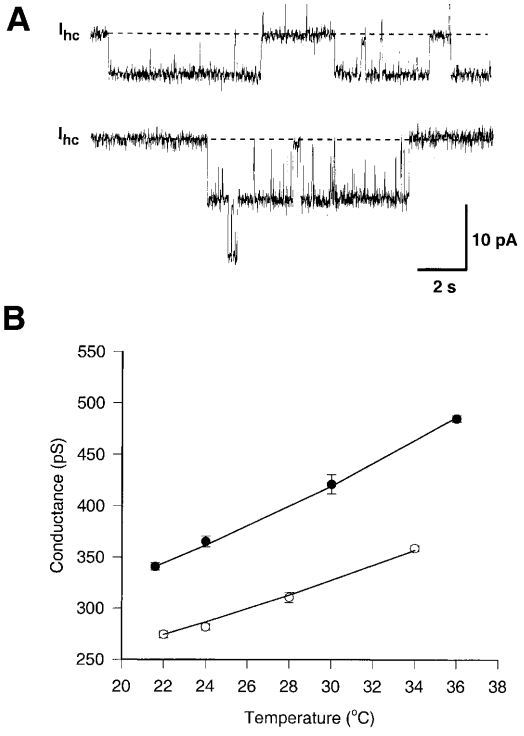

Fig. 10A, B Influence of temperature on single Cx30 hemichannels. **A** Examples of $I_{hc,main}$ records obtained at 22°C (*upper trace*) and 36°C (*lower trace*) elicited at V_m=–20 mV, yielding conductances of 320–334 pS and 460–486 pS, respectively. **B** Plots of $\gamma_{hc,main}$ data gained at V_m=–20 mV (•) and 30 mV (o) versus temperature, *T*. *Symbols* represent mean values ±1SEM. Curves correspond to the best fit of data to a single exponential. The temperature coefficient, Q_{10}, of $\gamma_{hc,main}$ at V_m=–20 and 30 mV was 1.28 and 1.25, respectively. Bath: Krebs-Ringer solution with no added Ca^{2+}, NaCl replaced by potassium aspartate

Figure 11A shows a family of I_{hc} records from a cell superfused with Ca^{2+}-free Krebs-Ringer containing KCl instead of NaCl. To reduce the number of operational hemichannels, 2 mM heptanol was added in some preparations. The dashed lines refer to $I_{hc,main}$. The traces indicate that the dwell time at discrete levels was dependent on V_m. At 50 mV, the channel flickered rarely and was seldom in the main state. At 40 mV, fast flickering was more frequent and the channel spent some time in the main state. At 30 mV, the channel flickered more rarely again but was preferentially in the main state. The currents associated with negative voltages, i.e., –12, –20 and –45 mV, revealed a mirror image. This suggests that Cx30 hemichannels close in a V_m-dependent manner at positive and negative voltage. The transitions between $I_{j,main}$ and $I_{j,residual}$ were always fast (see Fig. 6).

The currents in Fig. 11A disclose additional properties of Cx30 hemichannels. At small V_m, i.e., –12 and 30 mV, fast flickering occurred randomly whereas at large V_m, i.e., –20, –45, 40 and 50 mV, it was interrupted by prolonged periods in the residual state. Moreover, the I_{hc} signal at V_m=–45 mV showed a rare event, i.e., a slow transition between the residual state and closed state which lasted about 8 ms. Such transitions were usually

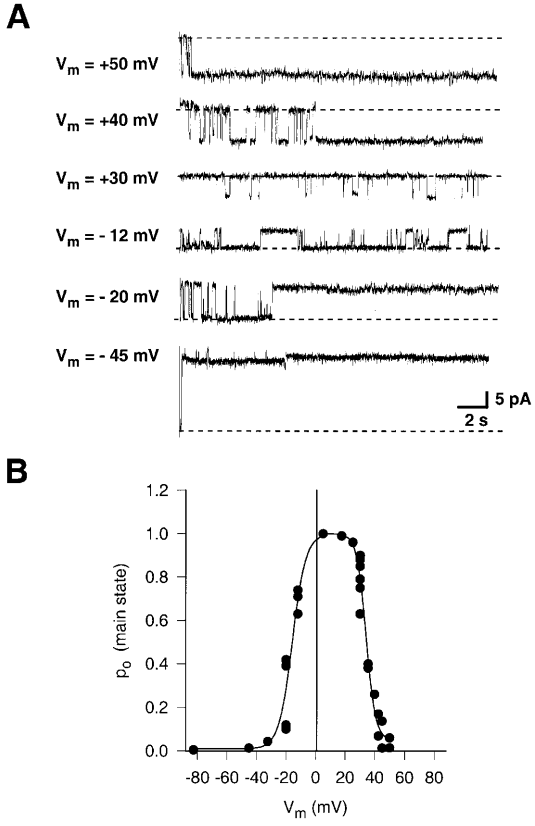

Fig. 11A, B Main-state probability. **A** Influence of membrane potential, V_m, on the activity of single Cx30 hemichannels. Family of current traces recorded at steady state, elicited by different V_m. *Dashed lines* refer to the main state. The *traces* indicate that the dwell time at discrete current levels is correlated with the amplitude of V_m. The frequency and duration the channel spent in the main state decreased with increasing $|V_m|$. **B** Voltage dependence of the main-state probability, P_o, of Cx30 hemichannels. Values of P_o were determined from long I_{hc} segments (>15 s) at steady state. The data were obtained from single channel records of three cells. Each *symbol* represents a single determination. *Smooth curves*: theoretical fit of data to the Boltzmann equation: $V_{m,0}$=–16/34 mV, $P_{o,min}$=0/0, z=5.6/7.9 for negative/positive V_m. Bath: Krebs-Ringer solution with no added Ca^{2+}, NaCl replaced by KCl

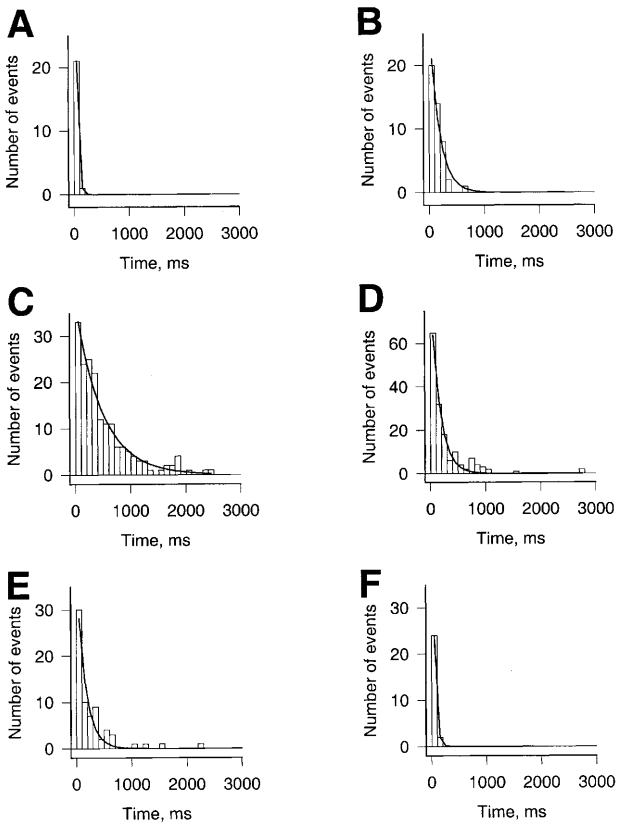

Fig. 12A–F Open time histograms of Cx30 hemichannels. Single-channel currents were analyzed for dwell times in the main state (i.e., channel open times) at different membrane potentials, V_m, at steady state. Data from three cells were sampled and plotted as frequency histograms. *Curves* correspond to the best fit of data to a single exponential: **A** τ_o=33 s (V_m=50 mV); **B** τ_o=173 s (V_m=40 mV); **C** τ_o=484 s (V_m=30 mV); **D** τ_o=158 s (V_m=-12 mV); **E** τ_o=156 s (V_m=–20 mV); **F** τ_o=40 s (V_m=–45 mV). Bath: Krebs-Ringer solution with no added Ca^{2+}, NaCl replaced by KCl

seen in conjunction with chemical uncoupling (see Fig. 8C, D). Since this event was observed long after washout of heptanol, it may reflect an unusual kind of physical gating rather than chemical gating [1, 22].

To determine P_o, the time a channel spent in the main state was measured and expressed as a fraction of record duration. Figure 11B shows the plot P_o versus V_m which includes the complete data from three cells. P_o was maximal at small V_m. It decreased in a sigmoidal manner from 1 and 0 when V_m was made more positive or negative. The data were fitted with the Boltzmann equation:

$$P_o = \frac{1 - P_{o,min}}{1 + e^{[A\cdot(V_m - V_{m,0})]}} + P_{o,min} \quad (4)$$

where $P_{o,min}$ is the minimal P_o at large V_m and $V_{m,0}$ corresponds to V_m at which P_o is half-maximal. The analysis yielded the following values: $V_{m,0}$=–16/34 mV, $P_{o,min}$=0/0, z=5.6/7.9 for negative/positive values of V_m, respectively.

Steady-state kinetics of single-channel currents

Cx30 hemichannels mainly flicker between the main state and residual state. To study the underlying processes, long I_{hc} records at steady state were used to analyze the channel dwell times. Substates were ignored because of rare occurrence and short duration. Figure 12 shows histograms of the open lifetime at V_m=50 (A), 40 (B), 30 (C), –12 (D), –20 (E) and –45 mV (F). The analysis involves data from three cells. The distributions of the open lifetimes were best approximated by single exponentials, indicating that a single main state is involved. Curve fitting yielded the following time constants τ_o: 33, 173, 484, 158, 156 and 40 s, respectively. The determination of channel closed times, i.e., the time spent in the residual state, was not satisfactory. On the one hand, the number of events was low, especially at small V_j. On the other hand, due to the limited response time of the exper-

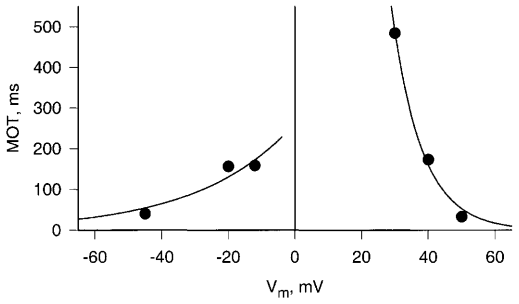

Fig. 13 Steady-state kinetics of Cx30 hemichannels. Channel mean open times (i.e., main state) were determined from the probability density function using the rate constants of channel closure, β, and plotted versus V_m. Curves correspond to the best fit of data to a single exponential with a decay constant of 28.6 and 9.0 for negative/positive V_m. Bath: Krebs-Ringer solution with no added Ca^{2+}, NaCl replaced by KCl

imental setup (1–2 ms), short lived residual states may have been confused with substates.

The curves fitted in Fig. 12 represent the probability density function $f(t)=\beta \cdot e^{-\beta t}$, where $1/\beta$ corresponds to the channel mean open time, i.e., the average time a channel spent in the main state. Figure 13 shows a plot of the mean open times derived in this way versus V_m. The smooth curves were obtained by fitting the data to an exponential with a decay constant of 28.7 and 9.0 for negative and positive V_m, respectively. The mean open time decreased with increasing $|V_m|$. This suggests that the channels stayed less frequently and/or for shorter times in the main state as $|V_m|$ was increased.

Conductances of gap junction channels versus hemichannnels

Does docking of hemichannels participate in determining the properties of gap junction channels? To answer this question, we carried out experiments with Cx30 hemichannels under conditions mimicking those used in a previous study on Cx30 gap junction channels (bath and pipette solution: potassium aspartate) [25]. The $\gamma_{hc,main}$ data gathered were sampled, averaged and plotted versus V_m. Figure 14A summarizes the results from six cells. Over the V_m range –70 to 55 mV, $\gamma_{hc,main}$ increased with hyperpolarization and decreased with depolarization (o). The solid curve represents the best fit of data to Eq. 2. The analysis furnished the following values: Γ_H=321 pS, V_H=–346 mV. The dashed curve corresponds to the $\gamma_{hc,main}=f(V_m)$ predicted from the experiments on Cx30 gap junction channels [25]. It was obtained by fitting the data to a mathematical model [26] considering the relationship between the conductance of a gap junction channel ($\gamma_{j,main}$) and its hemichannels (γ_{hc1}, γ_{hc2}):

$$\gamma_{j,main} = \frac{\gamma_{j,main(hc1)} \cdot \gamma_{j,main(hc2)}}{\gamma_{j,main(hc1)} + \gamma_{j,main(hc2)}} \quad (5)$$

The values of the parameters underlying the predicted curve were: Γ_H=291 pS, V_H=–253 mV. Although both

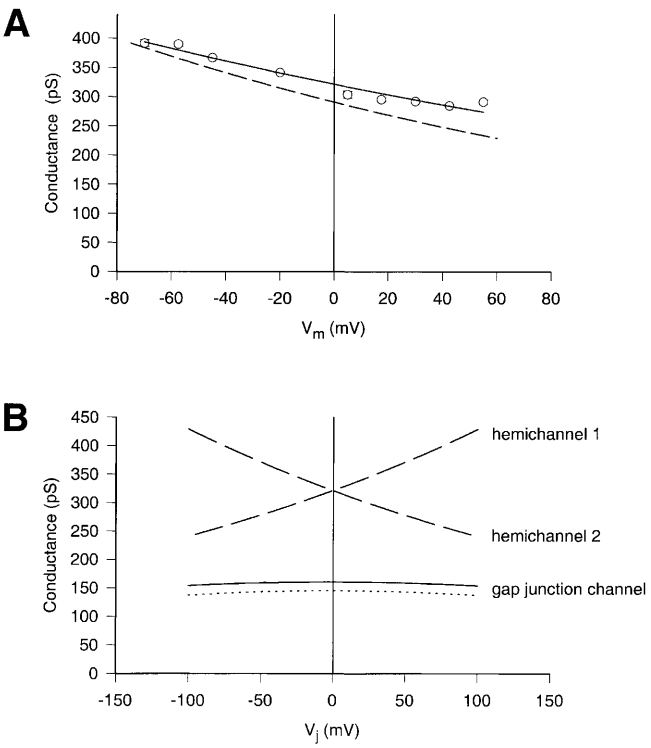

Fig. 14A, B Comparison of Cx30 hemichannnels and gap junction channels. **A** Plot of $\gamma_{h.c,main}$ determined from six cells versus V_m. *Symbols* are means ±1SEM. *Solid curve*: best fit of data to Eq. 2. *Dashed curve*: $\gamma_{hc,main}=f(V_m)$ predicted from experiments on Cx30 gap junction channels. Conditions: bath and pipette solution: potassium aspartate. **B** Synopsis of Cx30 data. *Dashed curves*: $\gamma_{hc,main}=f(V_m)$ of hemichannels hc1 and hc2, gained from hemichannel data. *Solid curve*: $\gamma_{j,main}=f(V_j)$ of a gap junction channel, deduced from hemichannel data using Eq. 5. *Dotted curve*: $\gamma_{j,main}=f(V_m)$ obtained from experiments on Cx30 gap junction channels using our mathematical model [25]

curves exhibit a V_m sensitivity, the predicted curve is slightly steeper and shifted towards smaller conductances. Hence, it appears that docking affects both the voltage sensitivity and the conductance.

Figure 14B presents a synopsis of the Cx30 conductance data. The dashed curves cross each other at V_m=0 mV and represent $\gamma_{hc,main}=f(V_m)$ for hc1 and hc2. They were gained from hemichannel experiments (see Fig. 14A). The solid curve corresponds to $\gamma_{j,main}=f(V_j)$ and describes the behavior of a gap junction channel. It is a theoretical curve since it was deduced from hemichannel data using Eq. 5. In contrast, the dotted curve shows the experimental $\gamma_{j,main}=f(V_m)$. It was obtained from experiments on Cx30 gap junction channels [25] and involved fitting of unitary conductance data to the mathematical model [26]. A comparison of the solid and dotted curve indicates that $\gamma_{j,main}$ at V_j=0 mV predicted from hemichannels is somewhat larger than the value determined experimentally, i.e., 160 versus 146 pS.

Discussion

Direct evidence for hemichannels has emerged from electrophysiological studies. The oocyte expression system has allowed the measurement of currents through hemichannels of identified connexins (multichannel currents: rat Cx46, chicken Cx56, *Xenopus* Cx38 [9, 10, 11]; single-channel currents: rat Cx46 [22]). The goal of the present study was to examine hemichannels in transfected HeLa cells expressing mouse connexins. Its success relies on (1) the presence of hemichannels in cell membranes, (2) the hemichannel density, and (3) a protocol to open silent hemichannels. With regard to (1) and (2), studies exploring the de novo formation of gap junctions suggested that hemichannels exist in the membrane of transfected HeLa cells, although at low density (e.g., [4]). With respect to (3), we adopted the protocol introduced for oocytes, i.e., lowering $[Ca^{2+}]_o$ and reducing V_m [10].

Identification of hemichannels

One way to identify membrane channels involves using specific blockers. Unfortunately, there are no such tools specific for gap junction channels. In the absence of a sole rigorous criterion, we resorted to a set of less stringent features. Separately, each of them may be ambiguous. In combination, they conclusively identify hemichannel currents unequivocally. It will be shown that the data gathered are consistent with the view that I_{hc} is mediated by hemichannels consisting of Cx30, Cx46 or Cx50.

Experimental conditions

In transfected HeLa cells, removal of extracellular Ca^{2+} induced a novel current, I_{hc}, apparent in multichannel and single-channel signals. I_{hc} disappeared when $[Ca^{2+}]_o$ was restored. This is consistent with the observation that cytosolic Ca^{2+} impairs gap junctions via chemical gating [27]. I_{hc} was only present at depolarized V_m. It disappeared with hyperpolarization. This is compatible with the mechanism of voltage gating of gap junction channels [4]. The involvement of chemical and voltage gating renders it likely that I_{hc} is carried by hemichannels.

Transfected cells versus wild-type cells

Removal of extracellular Ca^{2+} in conjunction with depolarization of V_m provoked an I_{hc} in HeLa cells expressing Cx30, Cx46 or Cx50, but not in wild-type cells. This suggests that I_{hc} is carried by channels introduced by transfection, conceivably hemichannels. However, HeLa cells also express an intrinsic connexin albeit at a marginal level, i.e., Cx45 [14]. Indeed, besides large unitary conductances, we observed small ones in a few cases (≅80 pS). Since they were V_m sensitive, they may reflect intrinsic hemichannels.

Intrinsic membrane channels

Wild-type HeLa cells express three membrane channels, two potassium and a chloride channel. Currents carried by these channels may be confused with hemichannel currents. However, their properties are easy to distinguish from those of I_{hc}. Potassium channels have a low conductance (10–40 pS), show inward rectification and are selective for K^+, one being Ca^{2+} dependent and voltage insensitive [20], the other one Ca^{2+} insensitive and voltage dependent [19]. The chloride channel has a low conductance (<5 pS), shows outward rectification and volume activation, and is anion selective [8, 19].

Chemical gating

Lipophilic agents, e.g., heptanol or SKF-525A, provoked a reversible decrease of I_{hc} in Cx30, Cx46 and Cx50 cells (see Fig. 8A,B). I_{hc} recorded late during wash in or early during washout of such agents provided insight into the underlying mechanisms. At the single-channel level, I_{hc} exhibited slow transitions (≅10 ms) between an open state (i.e., main state or residual state) and the fully closed state (see Fig. 8C, D). As a result, slow transitions starting from an open state terminated fast flickering, while slow transitions ending at an open state re-established fast flickering of a previously closed channel. Such events were absent without uncoupling agents (for an exception, see Fig. 11A). They resemble those seen in single gap junction channels exposed to lipophilic agents and hence are attributable to chemical gating [24, 27]. This similarity provides strong evidence that I_{hc} is carried by hemichannels.

Expression systems

I_{hc} in Cx46 transfected HeLa cells resembles the currents that are seen in Cx46-injected *Xenopus* oocytes and attributed to hemichannels. At the multichannel level, both expression systems yielded currents with time- and voltage-dependent inactivation (data not shown; [10, 11, 22]). At the single-channel level, both systems exhibited currents with a main state and residual state (see "Single channel properties"; [22]). These similarities support the view that I_{hc} is carried by hemichannels.

Hemichannels versus gap junction channels

Provided I_{hc} is a hemichannel current, it is possible to predict some of its properties from gap junction channel data: (1) With increasing voltage, $g_{hc,ss}$ is expected to decrease in a sigmoidal fashion without reaching zero. (2)

Hemichannels must exhibit a residual conductance state, $\gamma_{j,residual}$. (3) A non-linear relationship $\gamma_{hc,main}=f(V_m)$ is anticipated from the behavior of heterotypic gap junction channels. (4) $\gamma_{hc,main}$ can be estimated from $\gamma_{j,main}$ by means of Eq. 5. (5) The functions $P_o=f(V_m)$ and $P_o=f(V_j)$ which describe the kinetic behavior of hemichannels and gap junction channels respectively, are expected to resemble each other.

These aspects are crucial and merit more extensive discussion (see below). It will be shown that they are consistent with the hemichannel hypothesis.

Multichannel properties

For all three hemichannels studied, I_{hc} showed a time- and voltage-dependent inactivation irrespective of V_m polarity. This resulted in a nearly constant $g_{hc,inst}=f(V_m)$ and a bell-shaped $g_{hc,ss}=f(V_m)$. Gating of hemichannels with negative *and* positive V_m provokes a conflict since the operation of gap junction channels is considered to involve gating by positive *or* negative voltage of hemichannels [26]. Based on our data, we propose the following hypothesis. Gating of hemichannels with positive voltage controls the properties of gap junctions (V_j-gating) while gating with negative voltage affects the properties of cell membranes (V_m or "loop" gating [22]). Hence, under physiological conditions, i.e., $V_j \cong 0$ mV and negative V_m, gap junction channels are open and allow to co-ordinate the activity of cells in a tissue while unopposed hemichannels are closed completely and help to maintain the integrity of the cells. This concept is consistent with that derived from the behavior of Cx46 hemichannels expressed in oocytes [22].

A key finding was that $g_{hc,ss}=f(V_m)$ of Cx30 hemichannels is bell-shaped and asymmetrical. This means that unopposed hemichannels possess two different mechanisms of voltage gating. A comparison of the Boltzmann parameters $V_{hc,0}$ (–14.3/25.6 mV for negative/positive voltage) and $V_{j,0}$ (27 mV [25]) suggests that V_j gating of gap junction channels is governed by positive voltage. Hence, V_m or "loop" gating of unopposed hemichannels may be controlled by negative voltage. Other features were that I_{hc} of the hemichannels declines to a residual level while P_o approaches zero when V_m is strongly hyper- or depolarized (compare Figs. 3, 4 and 11B). These properties are reminiscent of gap junctions as previously shown for Cx30, Cx46 and Cx50 ([25]; V. Valiunas and R. Weingart, unpublished observations; R. Sakai, C. Elfgang, K. Willecke, R. Weingart, work in preparation). A comparison of $g_{hc,min}$ (0.14/0.35 for negative/positive voltage) and $g_{j,min}$ (0.15 [25]) for Cx30 implies that V_j gating is controlled by negative voltage. However, if one allows for a contribution of intrinsic membrane channels (see Fig. 3C), this leads to a $g_{hc,min}$ of about 0.06/0.2 for negative/positive voltage. This would also suggest that V_j gating is operated by positive rather than negative voltage. The notion that $g_{hc,min}$ reflects the residual state of hemichannels predicts a close match between $g_{hc,min}$ and $\gamma_{hc,residual}/\gamma_{hc,main}$. In the case of Cx30, this is true for positive voltage (0.2 and 0.17), but not for negative one (0.06 and 0.17). This is also consistent with the view that V_j gating of Cx30 channels involves positive voltage. The low $g_{hc,min}$ at negative voltage may also reflect a simultaneous involvement of V_m and V_j gating, i.e., V_j gating in unopposed hemichannels may operate at positive *and* negative voltage. This conclusion would be compatible with the observation that hemichannels also exhibit a residual conductance at negative voltage, attributable to V_j gating in gap junction channels. Moreover, since g_{hc} is zero at physiological conditions, we predict that Cx30 hemichannels possess a chemical gate which closes the channel completely in the presence of extracellular Ca^{2+}. Alternatively, extracellular Ca^{2+} may interfere with both the V_m gate *and* V_j gate to close the hemichannel. In essence, the conclusions derived from Cx30 hemichannel experiments also apply to Cx46 and Cx50 hemichannels.

Our multichannel data are consistent with the findings in studies of rat Cx46 hemichannels expressed in *Xenopus* oocytes. Initially, it had been reported that $g_{hc,ss}$ decreases in a S-shaped manner when V_m is hyperpolarized from 0 to –70 mV [10, 11]. Later on, it was found that $g_{hc,ss}$ declines with increasing negative *and* positive V_m [22].

Single channel properties

Channel conductances

I_{hc} exhibited two major single-channel conductances attributable to the main state and residual state. In between, short-lived substates were seen occasionally. The current transitions between these states were beyond the frequency response of the recording equipment (i.e. <1–2 ms). On rare occasions, slow transitions were seen between an open state (see above) and the closed state. This behavior was observed in Cx30, Cx46 and Cx50 HeLa cells. It suggests that V_m gating does not lead to complete hemichannel closure – extracellular Ca^{2+} is required to do so. These properties are consistent with those of the respective gap junction channels expressed in HeLa cells ([25]; V. Valiunas and R. Weingart, unpublished observations; R. Sakai, C. Elfgang, K. Willecke, R. Weingart, work in preparation). However, they contrast with those of rat Cx46 hemichannels expressed in *Xenopus* oocytes. In this preparation, depolarization leads to fast transitions between the open state and a substate, and hyperpolarization to slow transitions between the open state and closed state [22].

Our measurements yielded the following mean values for $\gamma_{hc,residual}$ and $\gamma_{hc,main}$: Cx30: 48 and 283 pS; Cx46: 37 and 250 pS; Cx50: 77 and 352 pS (pipette solution: potassium aspartate; bath solution: NaCl; extrapolated to V_m=0 mV). Hence, $\gamma_{hc,main}$ and $\gamma_{hc,residual}$ follow the sequence Cx46<Cx30<Cx50 as predicted from studies of gap junction channels ($\gamma_{j,residual}$ and $\gamma_{j,main}$: 19 and 128 pS

(R. Sakai, C. Elfgang, K. Willecke, R. Weingart, work in preparation), 25 and 146 pS [25] and 33 and 203 pS (V. Valiunas and R. Weingart, unpublished data); pipette solutions: potassium aspartate; data converted to T=23°C). Based on electrostatic principles, $\gamma_{hc,main}$ can be estimated from $\gamma_{j,main}$ [26]. It turns out that the $\gamma_{hc,main}$ measured and predicted are comparable to those for Cx30 (283 versus 291 pS) and Cx46 (250 versus 272 pS), but less so for Cx50 (352 versus 402 pS). However, it should be kept in mind that $\gamma_{hc,main}$ and $\gamma_{j,main}$ were gained with asymmetrical and symmetrical solutions, respectively (see above). In the case of Cx30, $\gamma_{hc,main}$ was also determined with symmetrical solutions, i.e. potassium aspartate. In this case, $\gamma_{hc,main}$ and $\gamma_{j,main}$ deviated considerably (measured: 321 pS; predicted: 291 pS), suggesting that hemichannel docking takes part in $\gamma_{j,main}$. For comparison, rat Cx46 hemichannels expressed in oocytes yielded a conductance of ≅300 pS and a subconductance of ≅100 pS (pipette solutions: 100 mM KCl; room temperature) [22].

Voltage sensitivity of $\gamma_{hj,main}$

The transfectants examined revealed a distinct V_m dependency of $\gamma_{hc,main}$. Hyperpolarization led to an increase in $\gamma_{hc,main}$, depolarization to a decrease (see Fig. 9). This behavior has been anticipated from the properties of heterotypic gap junction channels [5, 29]. Studies of pairs of Cx30-HeLa cells are also consistent with this finding [24, 25]. In this case, it ensues from the sum of the variable conductance of a gated hemichannel and the constant conductance of a non-gated hemichannel [26]. The function $\gamma_{hc,main}=f(V_m)$ varied among the hemichannels studied. Its steepness, characterized by V_H, followed the sequence Cx30>Cx50>Cx46 (–370, –121, –108 mV; pipette solution: potassium aspartate; bath solution: NaCl; Cx30, with potassium aspartate in the bath solution: –346 mV). Our gap junction model predicts a similar correlation for $\gamma_{hc,residual}$ [26]. However, our data were too scarce for such an analysis. The V_j sensitivity may arise from re-arrangement of charged amino acid residues located at the mouth of or inside the channel. Alternatively, cytoplasmic ions may screen surface charges of the channel proteins. For comparison, rat Cx46 hemichannels expressed in *Xenopus* oocytes also exhibit a voltage sensitivity [18, 22].

Open channel probability

Cx30 hemichannels yielded a bell-shaped and asymmetrical $P_o=f(V_m)$ (see Fig. 11B). Both branches declined from 1 to 0 in a sigmoidal fashion. Hence, $g_{hc,min}$ corresponds to $N\cdot\gamma_{hc,residual}$, N being the number of channels involved. The Boltzmann parameters deduced from single hemichannels, i.e., the P_o data ($V_{m,0}$=–16/34 mV, z=5.6/7.9 for negative/positive V_m), resemble those obtained from multiple hemichannels, i.e., the g_{hj} data ($V_{m,0}$=–14.3/25.6 mV, z=6.9/2.6; see Fig. 4). The respective parameters for Cx30 gap junction channels are as follows – single channels: $V_{j,0}$=37.5 mV, z=3; multiple channels: $V_{j,0}$=27 mV, z=4 [25]. A comparison of single and multichannel parameters leads to the following conclusions: (1) Gating of Cx30 hemichannels with positive voltage reflects V_j gating of gap junction channels; (2) Gating of hemichannels with negative voltage reflects V_m gating or "loop" gating , (3) Docking does not interfere with the polarity of gating of gap junction channels; (4) Functional cooperativity exists between gap junction channels and hemichannels (see [25]).

Channel lifetimes

Single channel records at steady state enabled us to construct channel lifetime histograms for Cx30 (see Fig. 12). It turned out that the open time distributions are best approximated by single exponentials. This implies that these hemichannels possess a single main state with regard to both V_j gating and loop gating. The time constant τ_o decreased from 484 to 33 ms when V_m was increased from 30 to 50 mV and decreased from 158 to 40 ms when V_m was increased from –12 to –45 mV. A comparison with the time constants τ_o of single Cx30 gap junction channels indicates that the latter are considerably larger [25]. This suggests that docking of hemichannels markedly slows down the kinetics of gap junction channels. Unfortunately, channel closed times could not be determined due to lack of data.

Acknowledgements The authors are indebted to Jenny Gygax for technical assistance and to Rolf Vogel for help in data analysis. The transfected cells were kindly provided by Dr. K. Willecke, Institute of Genetics, University of Bonn, Germany. The work was supported by the Swiss National Science Foundation (grants 31–45554.95 and 31–55297.98 to R.W.).

References

1. Banach K, Weingart R (2000) Voltage gating of Cx43 gap junction channels involves fast and slow current transitions. Pflügers Arch 439:248–250
2. Bruzzone R, White TW, Paul DL (1996) Connections with connexins: the molecular basis of direct intercellular signalling. Eur J Biochem 238:1–27
3. Bukauskas FF, Weingart R (1993) Temperature dependence of gap junction properties in neonatal rat heart cells. Pflügers Arch 423:133–139
4. Bukauskas FF, Elfgang C, Willecke K, Weingart R (1995) Biophysical properties of gap junction channels formed by mouse connexin40 in induced pairs of transfected human HeLa cells. Biophys J 68:2289-2298
5. Bukauskas FF, Elfgang C, Willecke K, Weingart R (1995) Heterotypic gap junction channels (connexin26 – connexin32) violate the paradigm of unitary conductance. Pflügers Arch 429:870–872
6. De Vries SH, Schwartz EA (1992) Hemi-gap junction channels in solitary horizontal cells of the catfish retina. J Physiol (Lond) 445:201–230
7. Díaz M, Sepúlveda FV (1995) Characterisation of Ca^{2+}-dependent inwardly rectifying K^+ currents in HeLa cells. Pflügers Arch 430:168–180

8. Díaz M, Valverde MA, Higgins CF, Rucareanu C, Sepúlveda FV (1993) Volume-activated chloride channels in HeLa cells are blocked by verapamil and dideoxyforskolin. Pflügers Arch 422:347–353
9. Ebihara L (1996) *Xenopus* connexin38 forms hemi-gap-junctional channels in the nonjunctional plasma membrane of *Xenopus* oocytes. Biophys J 71:742–748
10. Ebihara L, Steiner E (1993) Properties of a nonjunctional current expressed from a rat connexin46 cDNA in *Xenopus* oocytes. J Gen Physiol 102:59–74
11. Ebihara L, Berthoud VM, Beyer EC (1995) Distinct behavior of connexin56 and connexin46 gap junction channels can be predicted from the behavior of their hemi-gap-junctional channels. Biophys J 68:1796–1803
12. Evans WH, Ahmed S, Diez J, George CH, Kendall JM, Martin PEM (1999) Trafficking pathways leading to the formation of gap junctions. In: Novartis Foundation 219. Gap junction-mediated intercellular signalling in health and disease. Wiley, New York, pp 44–54
13. Foote CI, Zhou L, Zhu X, Nicholson BJ (1998) The pattern of disulfide linkages in the extracellular loop regions of connexin 32 suggests a model for the docking interface of gap junctions. J Cell Biol 140:1187–1197
14. Hülser DF, Rehkopf B, Traub O (1997) Dispersed and aggregated gap junction channels identified by immunogold labelling of freeze-fractured membranes. Exp Cell Res 233:240–251
15. Krisciukaitis A (1997) Computer programs for investigation of intercellular communication using double whole-cell voltage clamp. Electron Electric Engineer 4:71–83
16. Malchow RP, Qian H, Ripps H (1993) Evidence for hemi-gap junctional channels in isolated horizontal cells of the skate retina. J Neurosci Res 35:237–245
17. Nilius B, Sehrer J, Viana F, De Greef C, Raeymaekers L, Eggermont J, Droogmans G (1994) Volume-activated Cl^- currents in different mammalian non-excitable cell types. Pflügers Arch 428:364–371
18. Pfahnl A, Dahl G (1998). Localization of a voltage gate in connexin46 gap junction hemichannels. Biophys J 75:2323–2331
19. Sauvé R, Roy G, Payet D (1983) Single channel K^+ currents from HeLa cells. J Membr Biol 74:41–49
20. Sauvé R, Simoneau C, Monette R, Roy G (1986) Single-channel analysis of the potassium permeability in HeLa cancer cells: Evidence for a calcium-activated potassium channel of small unitary conductance. J Membr Biol 92:269–282
21. Schmilinsky-Fluri G, Valiunas V, Willi M, Weingart, R (1997) Modulation of cardiac gap junctions: the mode of action of arachidonic acid. J Mol Cell Cardiol 29:1703–1713
22. Trexler EB, Bennett MVL, Bargiello TA, Verselis VK (1996) Voltage gating and permeation in a gap junction hemichannel. Proc Natl Acad Sci USA 93:5836–5841
23. Valiunas V, Weingart R (1997) Voltage gating and conductive properties of gap junction hemichannels studied in transfected HeLa cells. In: Proceedings of 1997 International Gap Junction Conference, Key Largo, Florida, USA, July 12–17, 1997, p. 97
24. Valiunas V, Bukauskas FF, Weingart R (1997) Conductances and selective permeability of connexin43 gap junction channels examined in neonatal rat heart cells. Circ Res 80:708–719
25. Valiunas V, Manthey D, Willecke K, Weingart R (1999) Biophysical properties of gap junction channels formed by mouse connexin30 expressed in transfected HeLa cells. J Physiol (Lond) 519:631–644
26. Vogel R, Weingart R (1998) Mathematical model of vertebrate gap junctions derived from electrical measurements on homotypic and heterotypic channels. J Physiol (Lond) 510:177–189
27. Weingart R, Bukauskas FF (1995) Regulation of gap junctions by lipophilic agents and ions supports the concept of two gating mechanisms. Experientia 51:A68
28. Weingart R, Bukauskas FF (1998) Long-chain *n*-alkanols and arachidonic acid interfere with the V_m-sensitive gating mechanism of gap junction channels. Pflügers Arch 435:310–319
29. Weingart R, Bukauskas FF, Valiunas V, Vogel R, Willecke K, Elfgang C (1996). In: Proceedings of Keystone conference: molecular aspects of the function of intercellular junctions, p. 16. Lake Tahoe, Calif., USA, March 1–7, 1996